Journal of
Nanoscience and Nanotechnology
Vol. 7, 3624–3628, 2007

RESEARCH ARTICLE

Synthesis and Characterization of $LnPO_4 \cdot nH_2O$ (Ln = La, Ce, Gd, Tb, Dy) Nanorods and Nanowires

Weihua Di*, Xiaojun Wang, and Haifeng Zhao

Key Laboratory of Excited State Processes, Changchun Institute of Optics, Fine Mechanics and Physics, Chinese Academy of Sciences, Changchun 130033, People's Republic of China

Aqueous precipitation method has been used to synthesize lanthanide orthophosphates $LnPO_4 \cdot nH_2O$ (Ln = La, Ce, Gd, Tb, Dy) with high purity and yield. It has been shown by XRD, TGA, and FTIR characterization that the as-synthesized samples are the $LnPO_4$ hydrates ($LnPO_4 \cdot nH_2O$) with hexagonal rhabdophane-type structure. The X-ray diffraction peaks and absorption of PO_4^{3-} groups show a systematic shift from $LaPO_4 \cdot nH_2O$ to $DyPO_4 \cdot nH_2O$ due to the effect of lanthanide ionic contraction. The value of n in $LnPO_4 \cdot nH_2O$ depends on the lanthanide element and synthetic condition. Field-emission scanning electron microscopy observations show the morphology of as-synthesized samples, which consist entirely of nanorods/nanowires with diameters of 30–100 nm and lengths ranging from several hundreds of nanometers to several micrometers. The anisotropic growth of crystals should be responsible for the formation of nanorods/nanowires, which is related to the hexagonal crystal structure.

Keywords: Aqueous Precipitation, Rare Earth, Nanomaterials, Characterization, Luminescence.

1. INTRODUCTION

Recently, luminescent nanomaterials have attracted considerable attention due to their novel properties and potential applications in optoelectronic devices as active components.[1,2] Therefore, a variety of nanosized materials, including oxides, metal and alloys, semiconductors, metal chalcogenides, and polymers, and so forth have been synthesized and their physicochemical properties have also been extensively explored.[3–6] It has been shown that the physicochemical properties of nanomaterials are strongly associated with their sizes and morphology.[7–9] Especially, the optical properties of luminescent materials are strongly affected by their morphology. Therefore, controlled synthesis of luminescent nanostructures with desirable size and shape is still a great challenge.

Among the large number of lanthanide salts (oxides,[10] borates,[11] and fluorides,[12]) Lanthanide orthophosphates ($LnPO_4$) represent an important class of materials from academic as well as industrial points-of-view. Lanthanide orthophosphates possess a variety of favorable properties such as very high thermal stability (~2300 °C),[13] low solubility (Ksp = 10^{-25} to 10^{-27}) in water,[14] high refractive index ($n = 1.5$) and a high concentration of lasing ions (~1.8×10^{21} ions cm^{-3}).[15] Base on these properties, $LnPO_4$ can be used in a variety of applications, such as luminescent or laser materials, magnets, ceramics, catalysts, proton conductors, moisture sensors, heat-resistant materials, scintillators for X-ray and γ-ray detection in medical science, biochemical probes, and medical diagnostics.[16–18] Because of the importance of this class of materials, very recently, the preparation and characterization of lanthanide orthophosphates have received noticeable attraction. The reported methods for the synthesis of $LnPO_4$ commonly require higher temperature, high pressure, expensive precursors, or specific complexing agents or toxic agents.[19–21] In this work, a facile and efficient aqueous precipitation was adopted to synthesize the lanthanide orthophosphates, and the structure, morphology, and luminescent properties were characterized.

2. EXPERIMENTAL DETAILS

The samples were prepared by an aqueous precipitation method as follows. Appropriate amounts of high purity La_2O_3, Gd_2O_3, Tb_4O_7, and Dy_2O_3 were dissolved in concentrated HNO_3 to form La(III), Gd(III), Tb(III), and Dy(III) solutions, respectively. For the synthesis of $CePO_4$, $CeCl_3 \cdot 6H_2O$ was used as the reagent. Appropriate volume of $(NH_4)_2HPO_4$ solution was added slowly to above mentioned lanthanide(III) solutions under vigorous stirring. The final pH value was adjusted to 1–2 by the addition

*Author to whom correspondence should be addressed.

1533-4880/2007/7/3624/005 doi:10.1166/jnn.2007.847

of aqueous ammonia (NH_4OH). The mixtures are vigorously stirred for 12 h at 80 °C. The resulting products were washed using ethanol and distilled water, and centrifuged at 8000 rpm. This process was repeated several times, and then dried overnight at room temperature.

The XRD studies of all samples were performed on a Rigaku D/max-2000 X-ray powder diffractometer with a Cu target radiation resource ($\lambda = 1.54078$ Å). The operation voltage and current were fixed at 40 kV and 40 mA, respectively. The Fourier-transform infrared spectra (FTIR) of powders were recorded in the range of 600–4000 cm^{-1} on a fourier transform spectrometer (Perkin-Elmer, Spectrum 1, USA) with a resolution of 1 cm^{-1}. The powders were first mixed with KBr, then pressed into a cylindrical die. Thermogravimetric analysis (TGA) of powders coupled with differential thermal analysis (DTA) was performed up to 600 °C at the heating rate of 10 °C/min under nitrogen gas flow (TA instruments, model SDT 2960, USA). Field-emission scanning electron microscopic (FE-SEM) images were obtained with utilizing a Hitachi S-4800 scanning electron microscope. The excitation and emission spectra of the samples were measured at room temperature with a Hitachi F-4500 fluorescent spectrometer.

3. RESULTS AND DISCUSSION

The crystal structure of as-synthesized samples was identified by X-ray diffraction (XRD) analysis, as shown in Figure 1. The XRD patterns reveals that all the products are crystalline and isostructural. All the peaks can be well indexed to hexagonal rhabdophane-type $LnPO_4 \cdot nH_2O$ (Ln = La, Ce, Gd, Tb, Dy), compared with standard data file (see JCPDS card number shown in Fig. 1). Furthermore, XRD results show systematic shifts in the position of the diffraction peaks from La to Dy. For example, the (200) peak is systematically shifted to a large angle from $LaPO_4$ to $DyPO_4$, as indicated clearly in Figure 1.

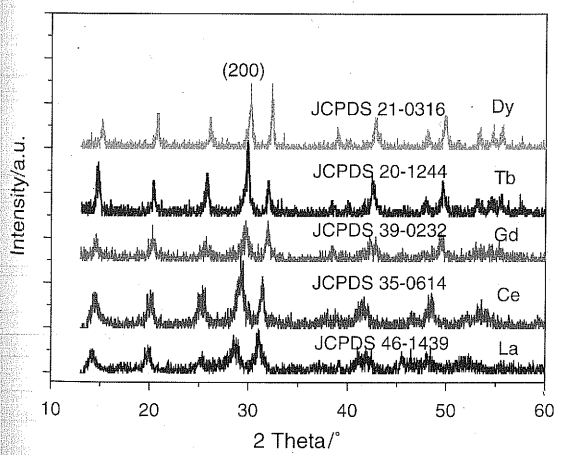

Fig. 1. XRD patterns of the as-synthesized $LnPO_4 \cdot nH_2O$ (Ln = La, Ce, Gd, Tb, Dy).

The systematic shift of the diffraction peaks is due to the difference in the lanthanide ion radii (the contraction of the ionic radii of the lanthanides). Also, it should be noted that the as-obtained lanthanide orthophosphates are commonly the hydrated compound. The hydration ratio depends primarily on the lanthanide ions, which is further characterized by TGA/DTA/FTIR measurements below.

FTIR spectra of as-synthesized hexagonal $LnPO_4 \cdot nH_2O$ are given in the range of 600–4000 cm^{-1}, as shown in Figure 2(a). The asymmetric wide bands between 3100 and 3700 cm^{-1} and the band at 1630 cm^{-1} are assigned to H_2O vibration. H_2O contained in these compounds mainly originates from the hydration water and the adsorption water from air, which have different characteristics. This difference can be identified by TGA/DTA measurements below. The band around 1400 cm^{-1} corresponds to the vibration of NO_3^- groups due to their adsorption at the surface of as-synthesized sample, which originate from the starting reactants ($LnNO_3$). Several attempts to remove these residuals completely by successive water-washing steps were unsuccessful. The rest bands in the investigated range of wave numbers are the characteristic vibrations of PO_4^{3-} groups. Take example for $LaPO_4 \cdot nH_2O$,

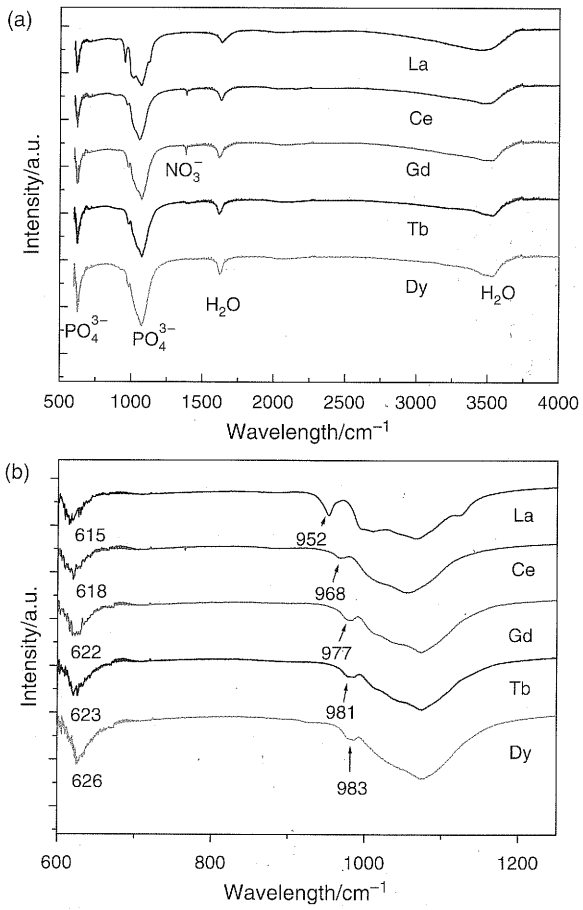

Fig. 2. FTIR spectra of the as-synthesized $LnPO_4 \cdot nH_2O$ (Ln = La, Ce, Gd, Tb, Dy) in the range 600–4000 cm^{-1} (a) and enlarged FTIR spectra in the range 600–1250 cm^{-1} (b).

the band at 615 cm^{-1} belongs to the v_3 vibration of the PO_4^{3-} groups; the should at 952 cm^{-1} corresponds to v_1 vibration and those located at 1015 and 1050 cm^{-1} are assigned to v_4 vibration (see Fig. 2(b)). No other phosphorus-containing groups such as $P_2O_7^{4-}$ (typically located at 1265–1267 cm^{-1}) are observed,[15] showing high purity of the as-synthesized samples. It is worth noting that there is an evident shift in the absorption frequencies in the different lanthanide orthophosphates. For example, the absorption peak at 952 cm^{-1} for $LaPO_4 \cdot nH_2O$ has been systematically shifted to that at 983 cm^{-1} for $DyPO_4 \cdot nH_2O$, as indicated in Figure 2(b). For other vibrations of PO_4^{3-} groups, the similar shifts are also observed. This systematic frequency shifts is also due to the effect of the lanthanide contraction,[22] consistent with the results obtained from XRD.

Typical TGA and DTA plots of as-synthesized $LaPO_4 \cdot nH_2O$ and $TbPO_4 \cdot nH_2O$ are given in Figure 3. For $LaPO_4 \cdot nH_2O$, two weight losses occur in two distinct steps with an overall weight loss of 7% from 40 °C to 600 °C. The first one occurs in the temperature range 60–150 °C, and is assigned to the release of residual water adsorbed at the powder surface due to the storage in air condition. Accordingly, it corresponds to a broad endothermic peak in the DTA curve in the temperature range 60–150 °C. The second weight loss (3.5%) begins at about 175 °C and finishes at 600 °C; this corresponds to the dehydration of the hydrated hexagonal $LaPO_4$. Also, a corresponding well-defined endothermic peak is observed in DTA curve in the temperature range 175–250 °C with a sharp peak at 220 °C. The weight loss of 3.5% resulting from the dehydration means about 0.5 mol hydration water in the $LaPO_4 \cdot nH_2O$. For $TbPO_4 \cdot nH_2O$, similar phenomena are observed from TGA/DTA curves. But the obvious differences in the dehydration weight and endothermic intensity are found. This indicates different hydration ratio in the different $LnPO_4 \cdot nH_2O$. By calculation, the value of n in $TbPO_4 \cdot nH_2O$ is close to 1. Interestingly, these samples after dehydration still maintains their original crystal structure. This therefore corresponds to the following equilibrium: $[LnPO_4 \cdot nH_2O]_{hexagonal} \rightarrow [LnPO_4]_{hexagonal} + nH_2O_{(gas)}$ (Ln = La, Ce, Gd, Tb, Dy).

The morphology of the as-synthesized samples was examined with field emission scanning electron microscopy (FE-SEM). Typical FE-SEM images of the samples are shown in Figure 4. The as-synthesized $LnPO_4 \cdot nH_2O$ (Ln = La, Ce, Gd, Tb, Dy) samples consist almost entirely of nanorods/nanowires with diameters of 30–100 nm and lengths ranging from several hundreds of nanometers to several micrometers. Differently, $TbPO_4$ nanowires are self-organized into a bundle-like structure. From these images, it is clearly observed that the synthesized nanorods/nanowires have been densely placed, meaning a high yield. Currently, the exact mechanism for the formation of $LnPO_4 \cdot nH_2O$ nanorods/nanowires has not been well known. Several researchers considered that the specific crystal structure is an inherent factor determining the morphology of synthesized samples.[23] The $LnPO_4 \cdot nH_2O$ synthesized in this work have a hexagonal crystal

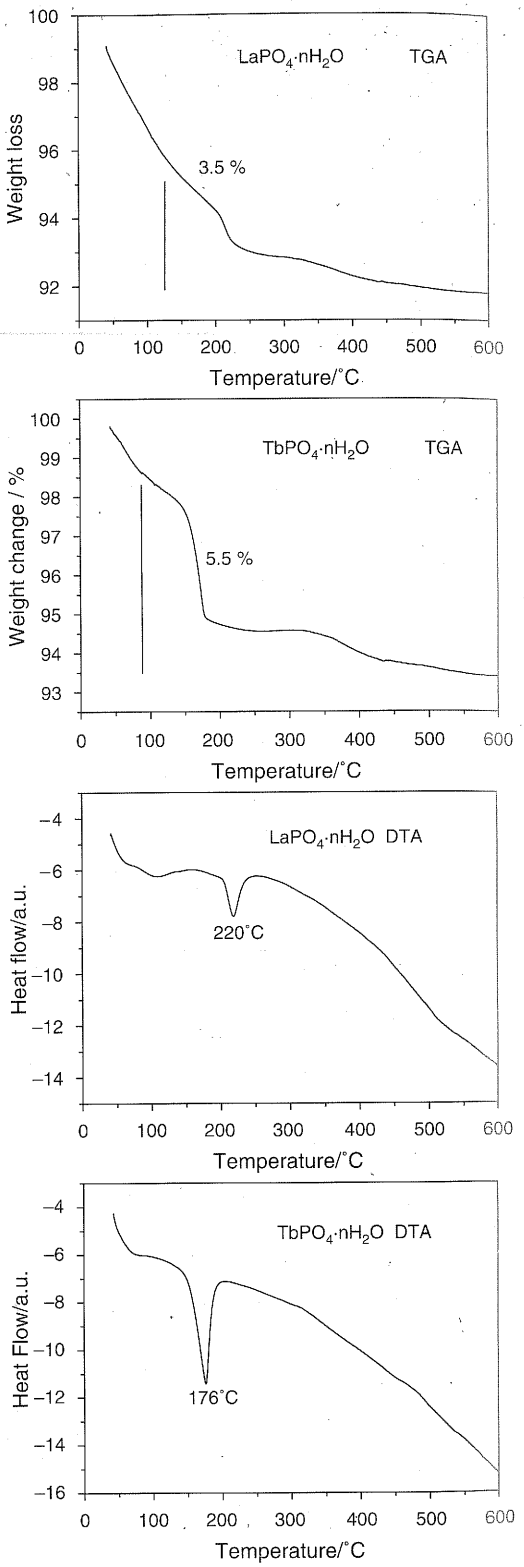

Fig. 3. Typical TGA/DTA curves of the as-synthesized $LaPO_4 \cdot nH_2O$ and $TbPO_4 \cdot nH_2O$.

(a) $LaPO_4 \cdot 0.5H_2O$

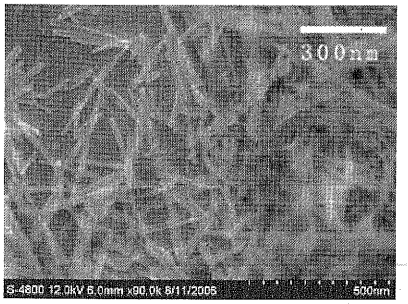

(b) $CePO_4 \cdot H_2O$

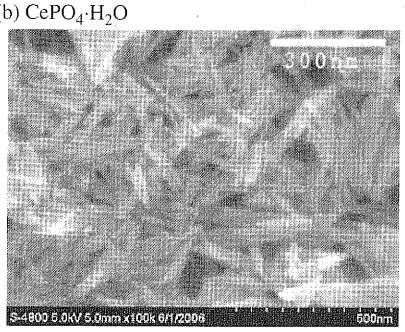

(c) $GdPO_4 \cdot H_2O$

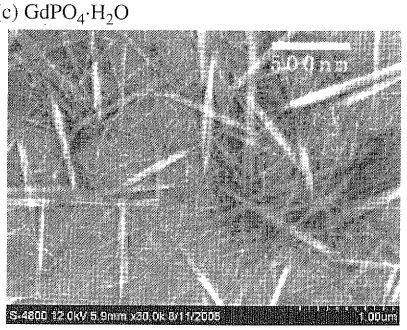

(d) $TbPO_4 \cdot H_2O$

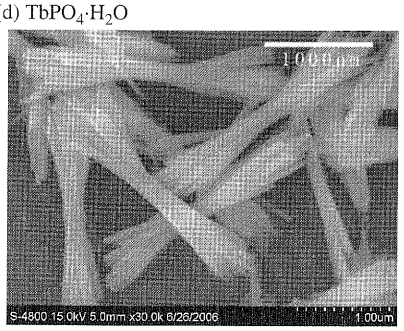

(e) $DyPO_4 \cdot 1.5H_2O$

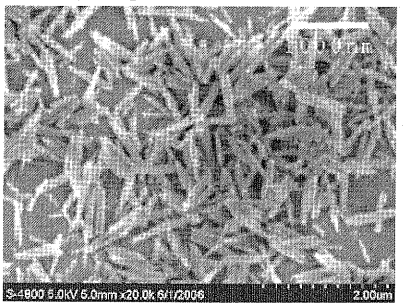

Fig. 4. FE-SEM micrographs of $LnPO_4 \cdot nH_2O$ (Ln = La, Ce, Gd, Tb, Dy).

structure, similar to that of ZnO and $Ln(OH)_3$, which are known to exhibit anisotropic growth.[23] In principle, the anisotropic growth of a crystal should contribute to the formation 1D nanomaterials.

The luminescent properties of undoped and doped rare earth nanomaterials have been widely investigated in the past several years. In 1999, Meyssamy et al.[19] first synthesized $LaPO_4$:Eu and $LaPO_4$:Tb nanoparticles (NPs) and nanowires (NWs), and characterized their luminescent properties simply. Yu et al.[24] further described the spectral properties of $LaPO_4$:Eu NPs and NWs, and especially revealed the difference of luminescent properties between NPs and NWs and the origin of this difference. However, the optical properties of the hydrated rare earth compounds have been studied rarely. The excitation and emission spectra of $CePO_4 \cdot 1H_2O$ nanorods are shown in Figure 5(a). It can be seen that the excitation bands consist of three components, having peaks at 256, 275, and 298 nm, respectively. These peaks are associated with allowed f–d transitions from the ground-state $^2F_{5/2}$ to different crystal-field components of the 5d level. A broad emission band centered at 350 nm corresponds to the transitions from the lowest 5d excited state to the spin-orbit components (^2D) of the doublet ground state, $^2F_{5/2}$ and $^2F_{7/2}$. A overlap between the emission band and excitation indicates a possibility of self reabsorption. The excitation

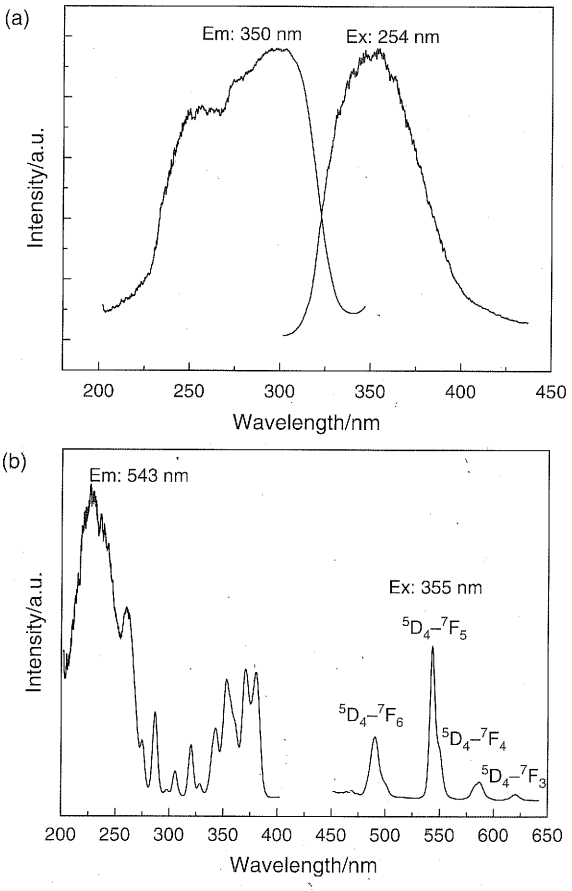

Fig. 5. Excitation and emission spectra of $LnPO_4 \cdot nH_2O$ (Ln = Ce, Tb).

Table I. The structure, morphology, water content, and yield of $LnPO_4 \cdot nH_2O$ (Ln = La, Ce, Gd, Tb, Dy).

$LnPO_4 \cdot nH_2O$	Crystal structure	Lattice constants a	Lattice constants c	Length (nm)	Width (nm)	Shape	Yield (wt%)
$LaPO_4 \cdot 0.5H_2O$	Hexagonal	7.100	6.494	200–300	30–40	Nanowires	95.3
$CePO_4 \cdot 1H_2O$	Hexagonal	6.960	6.372	150–200	30–40	Nanorods	93.6
$GdPO_4 \cdot 1H_2O$	Hexagonal	6.905	6.325	500–1000	20–100	Nanowires	98.4
$TbPO_4 \cdot 1H_2O$	Hexagonal	6.870	6.33	2000	50	Nanowires	97.8
$DyPO_4 \cdot 1.5H_2O$	Hexagonal	6.860	6.32	500	100	Nanorods	96.2

and emission spectra of $TbPO_4 \cdot 1H_2O$ nanowires are shown in Figure 5(b). For the excitation spectrum, the broad spectral lines are ascribed to the transition of the lower energy level of the $4f^8$ configuration to the energy levels of the $4f^75d$ configuration of the Tb^{3+}; the sharp spectral lines are assigned to the 4f–4f transitions of Tb^{3+}. Upon excitation of Tb^{3+} at 355 nm, the characteristic emissions of Tb^{3+} are observed due to the transitions of $^5D_4 - ^7F_j$ with the green emission at 543 nm being the most intense band.

4. CONCLUSIONS

We have successfully synthesized hexagonal rhabdophane-type $LnPO_4 \cdot nH_2O$ nanorods/nanowires with diameters of 30–100 nm and lengths ranging from several hundreds of nanometers to several micrometers. The structure, morphology, water content, and yield in the as-synthesized $LnPO_4 \cdot nH_2O$ are shown in Table I in detail. The formations of nanorods/nanowires are generally believed to relate to the hexagonal crystal structure, which is inherent force for the anisotropic growth of crystals. The value of n in $LnPO_4 \cdot nH_2O$ depends on the lanthanide ions ($n = 0.5$ for La, $n = 1$ for Ce, Gd, Tb, $n = 1.5$ for Dy). These $LnPO_4$ hydrates start to dehydrate at a certain temperature depending on the lanthanide ions, but still maintain original structure and morphology after dehydration. The X-ray diffraction peaks and characteristic absorptions of PO_4^{3-} groups show the systematic shift from $LaPO_4 \cdot nH_2O$ to $DyPO_4 \cdot nH_2O$ due to the effect of lanthanide ionic contraction.

Acknowledgments: This work was financially supported by the National Natural Science Foundation of China (Grant No. 50502031, 50572102), and Outstanding Young People Foundation of Jilin Province (Grant No. 20040113).

References and Notes

1. M. Huang, S. Mao, H. Feick, H. Yan, Y. Wu, H. Kind, E. Weber, R. Russo, and P. Yang, *Science* 292, 1897 (**2001**).
2. X. Duan, Y. Huang, Y. Cui, J. Wang, and C. M. Lieber, *Nature* 409, 66 (**2001**).
3. D. Zhang, L. Sun, J. Yin, and C. Yan, *Adv. Mater.* 15, 1022 (**2003**).
4. C. J. Murphy and N. R. Jana, *Adv. Mater.* 14, 80 (**2002**).
5. C. Yang, D. D. Stucky, and G. D. Stucky, *Chem. Mater.* 14, 1277 (**2002**).
6. M. Fu, Y. Zhu, R. Tan, and G. Shi, *Adv. Mater.* 13, 1874 (**2001**).
7. N. Pinna, K. Weiss, J. Urban, and M. P. Pileni, *Adv. Mater.* 13, 261 (**2001**).
8. W. Di, X. Wang, B. Chen, S. Lu, and X. Ren, *Appl. Phys. Lett.* 88, 011907 (**2006**).
9. V. F. Puntes, K. M. Kroshnan, and A. P. Alivisatos, *Science* 291, 2115 (**2001**).
10. D. Williams, B. Bihari, and B. Tissue, *J. Phys. Chem. B* 102, 916 (**1998**).
11. Z. Wei, L. Sun, C. Liao, J. Yin, X. Jiang, C. Yan, and S. Lu, *J. Phys. Chem. B* 106, 10610 (**2003**).
12. X. Wang and Y. D. Li, *Chem. Eur. J.* 9, 5627 (**2003**).
13. Y. Hikichi and T. Nomura, *J. Am. Ceram. Soc.* 70, C-252 (**1987**).
14. F. H. Firsching and S. N. Brune, *J. Chem. Eng. Data* 36, 93 (**1991**).
15. C. Para, G. Alexandra, S. Patra, D. Jacob, A. Gedanken, A. Landau, and Y. Gofer, *New J. Chem.* 29, 733 (**2005**).
16. W. Di, X. Wang, B. Chen, S. Lu, and X. Zhao, *J. Phys. Chem. B* 109, 13154 (**2005**).
17. S. Nishihama, T. Hirai, and I. Komasawa, *J. Mater. Chem.* 12, 1053 (**2002**).
18. E. Ordone-Rigil, R. drot, E. Simoni, and J. J. Ehrhardt, *Langmuir* 18, 7977 (**2002**).
19. H. Meyssamy, K. Riwotzki, A. Kornowski, S. Naused, and M. Haase, *Adv. Mater.* 11, 840 (**1999**).
20. J. M. Nedelec, C. Mansuy, and R. Mahiou, *J. Mol. Struct.* 165, 651 (**2003**).
21. M. Cao, C. Hu, Q. Wu, C. Guo, Y. Qi, and E. Wang, *Nanotechnology* 16, 282 (**2005**).
22. Y. P. Fang, A. W. Xu, R. Q. Song, H. X. Zhang, L. P. You, J. C. Yu, and H. Q. Liu, *J. Am. Chem. Soc.* 125, 16025 (**2003**).
23. X. Wang and Y. D. Li, *Angew. Chem. Int. Ed.* 41, 4790 (**2002**).
24. L. X. Yu, H. W. Song, S. Z. Lu, Z. X. Liu, L. M. Yang, and X. G. Kong, *J. Phys. Chem. B* 108, 16697 (**2004**).

Received: 22 January 2007. Revised/Accepted: 13 March 2007.